JOURNAL OF APPLIED POLYMER SCIENCE VOL. 19, PP. 1701–1722 (1975)

The Effect of Skin-Core Morphology on the Impact Fracture of Poly(butylene Terephthalate)

S. Y. HOBBS and C. F. PRATT, *Synthesis and Characterization Branch, Chemical Laboratory, General Electric Corporate Research and Development, P.O. Box 8, Schenectady, New York 12301*

Synopsis

Variations in the skin–core morphologies of injection-molded poly(butylene terephthalate) samples have been characterized as a function of molding conditions by optical microscopy, x-ray diffraction, and density measurements. Samples molded from 450 and 510°F melts at mold temperatures ranging from 70 to 250°F were found to have nonspherulitic skins whose thicknesses varied inversely with processing temperature. Very little orientation was observed in the skin or core regions of the molded bars. Density profiles are presented.

Impact data obtained on bars with molded-in notches demonstrate that significant increases in impact strength are observed with increasing skin thickness, although the maximum skin thickness remains less than a few hundred microns. This behavior persists through the ductile–brittle transition which is centered at ~50°C.

Fracture surface micrographs and high-speed stress–strain curves are presented and used to give a qualitative description of the fracture process. At room temperature the samples appear to deform elastically up to the point of fracture, while at higher temperatures extensive shear deformation is observed. In each case failure ultimately occurs via a craze–crack mechanism.

INTRODUCTION

Characteristic skin–core morphologies are known to develop in crystalline polymers during extrusion or injection molding. The structural details depend on the material, its rheological and crystallization characteristics, the location of T_g, and processing variables.[1] These features have been described in some detail for a number of crystalline polymers including polybutene-1,[2] nylon,[3] polypropylene,[4,5] and polyacetal.[6,17] Such studies are of great technological importance since the mechanical properties of an engineering thermoplastic are highly sensitive to morphological changes produced on molding.

In spite of general interest in this area there has been relatively little concern with the effect of skin–core morphology on the impact strength of injection molded parts. Kantz et al.[5] have reported some increase in the notched Izod strength of polypropylene with increasing skin thickness, but only when the skin was more than 60% of the total sample thickness. The enhanced impact strength was attributed to biaxial orientation in the shear zone without further explanation. Other studies have focused only on the variation of impact strength with overall levels of sample crystallinity with no mention of specific skin–core effects.[8]

We wish to report herein some recent investigations into the morphology and impact fracture characteristics of injection-molded poly(butylene terephthalate). For these studies we have employed impact bars with molded-in rather than cut notches. In these samples, in contrast to those which are notched after molding, the surface skin extends completely around the notch tip. This configuration offers two primary advantages: (*1*) it more closely approximates the character of commercial articles which are commonly fabricated with molded rather than cut notches and (*2*) it allows one to observe changes in impact strength which arise from thin, mechanically dissimilar surface skins which extend across the region of maximum stress concentration below the notch tip.

EXPERIMENTAL

Sample Preparation

Samples were fabricated from poly(butylene terephthalate) (PBT) obtained from the G. E. Plastics Division in Pittsfield, Massachusetts. The material was designated Valox 310 Thermoplastic Polyester Resin and had a melt viscosity of 7960 P at 480°F. The intrinsic viscosity in hexafluoroisopropanol at 25°C was $[\eta]^{25°C}_{HFIP} = 1.314$ dl/g.

Molding was done on a Battenfeld 0.8-oz injection-molding machine equipped with a doubly notched mold insert as shown in Figure 1. By cutting the specimen in half, two impact bars meeting ASTM D256 specifications were obtained. A 20-sec cycle time and 725-psi injection pressure were used for all samples. In the first run the barrel temperature was fixed at 450°F and the mold temperature was varied from 70 to 250°F. In the second run the barrel temperature was increased to 510°F. The samples are hereafter designated by their respective melt and mold temperatures (i.e. 450/70, 510/194, etc.).

Optical microscopy was carried out on a Zeiss WL polarizing microscope. Thin (5μ) sections were cut on a Porter Blum MT-2 ultramicrotome equipped

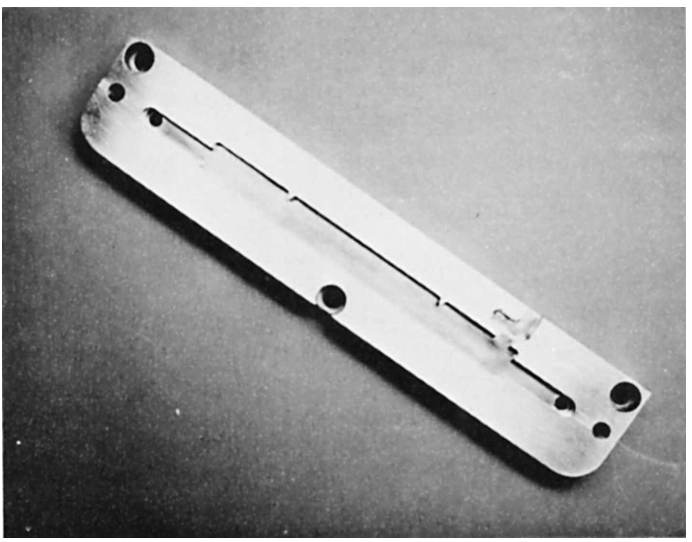

Fig. 1. Mold insert for producing two notched bars for Izod impact testing.

with a diamond knife. The samples were held in a liquid nitrogen cooled block to minimize distortion during slicing.

Scanning electron microscopy was performed on a JEOL JX A50A SEM. Prior to observation the samples were gold coated in a vacuum evaporator equipped with a rotary sample holder.

Transmission electron microscopy was carried out on a Siemens Elmiskop 101 microscope. Samples were prepared using both one- and two-stage replication techniques. In the first, the sample was rotary shadowed with platinum at 20° and backed with carbon. The direct replica was then removed by dissolving the polyester in hexafluoroisopropanol. In the second method, a cellulose acetate replica of the surface was prepared using acetone as a solvent. Platinum-shadowed carbon replicas were then prepared from the acetate film as described in the one-stage process. No differences were observed in samples prepared by the alternate methods.

Density Measurements

All density measurements were made in an aqueous KI density gradient column[9] at a temperature of 23 ± 0.2°C. The salt solution was degassed for ~1 hr under house vacuum to prevent air bubbles from collecting on the samples. Calibration with ASTM floats showed the column was linear over the density range 1.27–1.32 g/cm³. Sample densities were easily measured with a cathetometer to ±0.0002 g/cm³.

X-Ray Diffraction, Sonic Modulus, and Refractive Index Studies

X-Ray diffraction patterns were obtained on a GE XRD-5 x-ray unit using CuK_α radiation and a pinhole collimator. Samples were cut from the skin and core regions of the bars both parallel and perpendicular to the flow direction.

Refractive index and sonic modulus measurements were made directly on the molded bars using an Abbe refractometer and a Morgan PPM-5 dynamic modulus tester. The first technique samples a thickness of 0.5 μ, the latter 5–10 μ.

Impact Studies

Notched Izod impact tests were done on a Baldwin impact tester using a 2-lb hammer. In the high-temperature tests the samples were covered with a large, electrically heated copper block and allowed to equilibrate for 10 min. The cover was removed and the sample was struck. As the samples became increasingly ductile the hammer weight was increased to 4 lb. The data were appropriately corrected for windage and friction.

High-speed stress–strain data were collected on a specially designed MTS testing machine available in our laboratory. With this instrument it was possible to obtain stress–time profiles for samples impacted at velocities up to 8.3 ft/sec. From these curves the maximum load, elongation, and energy to break could be calculated directly.

The tests were conducted using a modified Charpy test configuration as shown in Figure 2. The hydraulically activated lower support was displaced $1/2$ in. from the ram nose prior to each run to assure that full test speed was attained. A rather severe ring which developed in the ram at the highest speeds was largely eliminated by inserting a suitable damping material beneath the load cell. This addition had no measurable effect on the output signal.

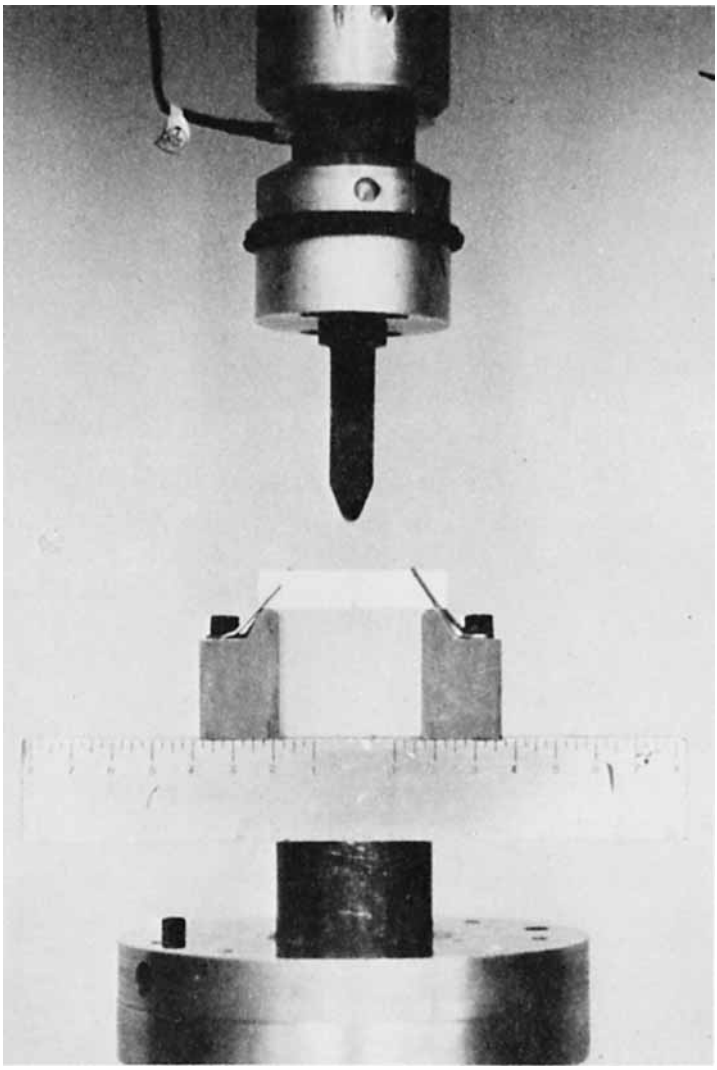

Fig. 2. Test configuration for high-speed fracture studies. The lower support forces the test piece up against the ram.

RESULTS

Skin–Core Morphology

Thin sections were microtomed from bars molded at different melt and mold temperatures from observation in the optical microscope. For a given sample no differences were observed in sections cut parallel or perpendicular to the flow direction or at various distances from the gate. All bars showed nonspherulitic skins which increased in thickness with decreasing melt and mold temperatures. These variations are shown in Table I. Isolated spherulites increasing in size from less than 1 μ to approximately 7 μ formed a poorly defined transition zone between the skin and core regions. The spherulites in the core zone were volume filling and reached a maximum diameter of 15 μ. The familiar Maltese cross ex-

TABLE I
Optical Skin Thicknesses in Injection-Molded Poly(butylene Terephthalate) Samples

Melt temperature, °F	Mold temperature, °F	Skin thickness, λ
450	70	202 ± 10
	122	149
	194	70
	250	33
510	70	178
	122	137
	194	66
	250	20

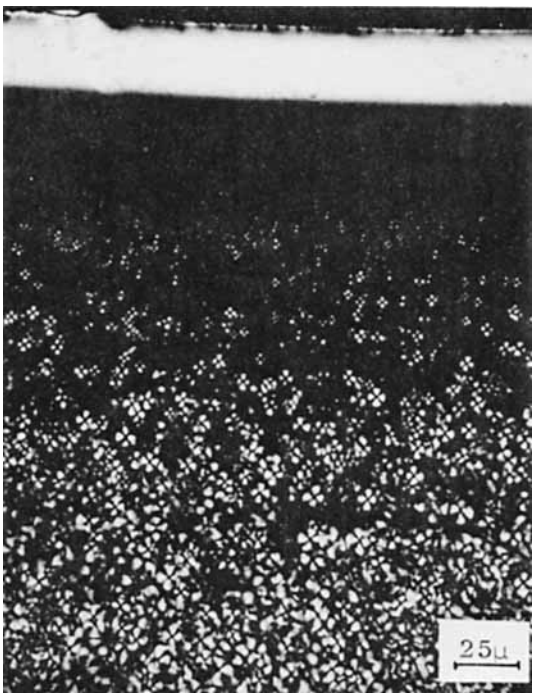

Fig. 3. Optical micrograph, crossed polarizers of a thin section cut from PBT Sample 450/122. The nonspherulitic skin, transition zone, and core region are shown. The birefringent region on the outer edge of the skin is a compression band formed during microtoming.

tinction pattern was oriented at 45° to the polarization direction. There was no evidence of anisotropic radial growth even in spherulites closest to the skin, indicating the degree of orientation in this region was low. The various morphological features are visible in Figure 3.

The very low degree of orientation in the skin and the absence of a subsurface shear zone contrasts with the observations of other investigators on polypropylene and polyacetal.[5,6] Significantly, x-ray diffraction photographs (see below) and sonic modulus measurements showed a similar lack of orientation in the molded bars. Refractive index measurements which are more sensitive to surface effects, however, reveal that $\eta_x \cong \eta_y < \eta_z$ (see Fig. 4), demonstrating that

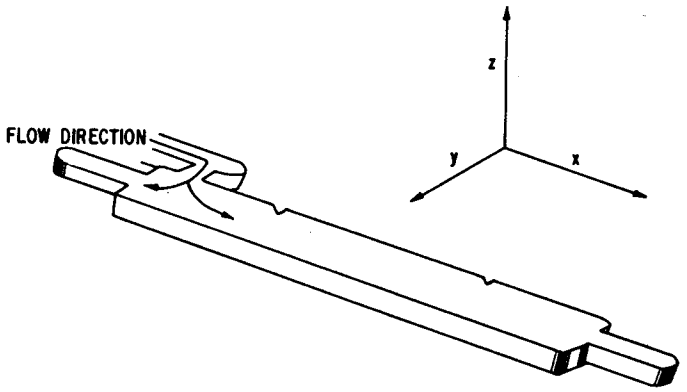

Fig. 4. Principle axes of injection-molded bar with respect to flow direction.

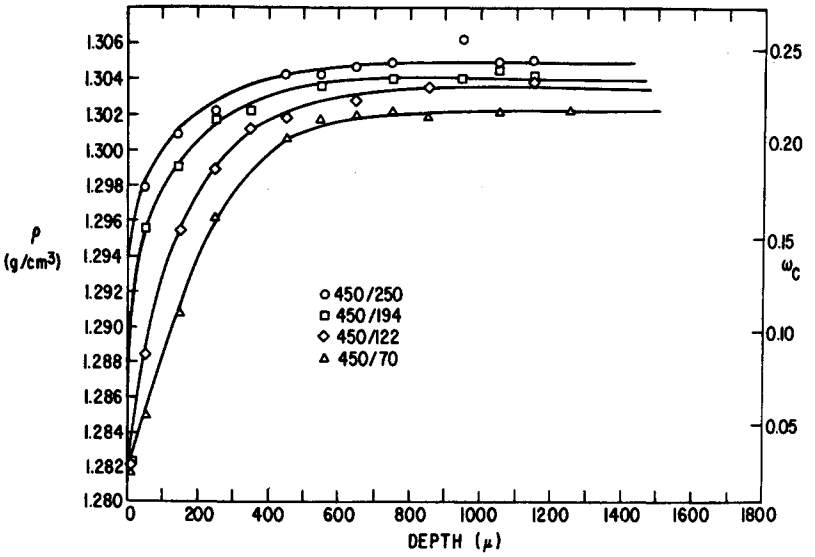

Fig. 5. Densities of injection-molded PBT bars at various distances from their outer surfaces as a function of mold temperature.

there is some anisotropic character to the material on the very outside of the moldings. A more exact determination of molecular orientation in this region awaits determination of the appropriate stress and strain optical coefficients of the material. The low level of orientation observed in the skin is indicative of rapid stress relaxation in the low viscosity melt during cooling.

Density profiles for bars molded at each temperature were constructed from measurements on 50 μ sections cut from the skin toward the core. These data are presented graphically in Figure 5 for bars molded from the 450°F melt. In contrast to the relatively abrupt skin–core boundaries observed in the optical microscope, the densities of all samples were found to increase continuously to a depth of 600 μ. The ultimate core densities were found to be relatively insensitive to mold temperature ranging from 1.302 g/cm^3 for sample 450/70 to 1.305 g/cm^3 for sample 450/250. In contrast, increasingly larger density differences among the samples were observed near the surfaces with all densities falling off

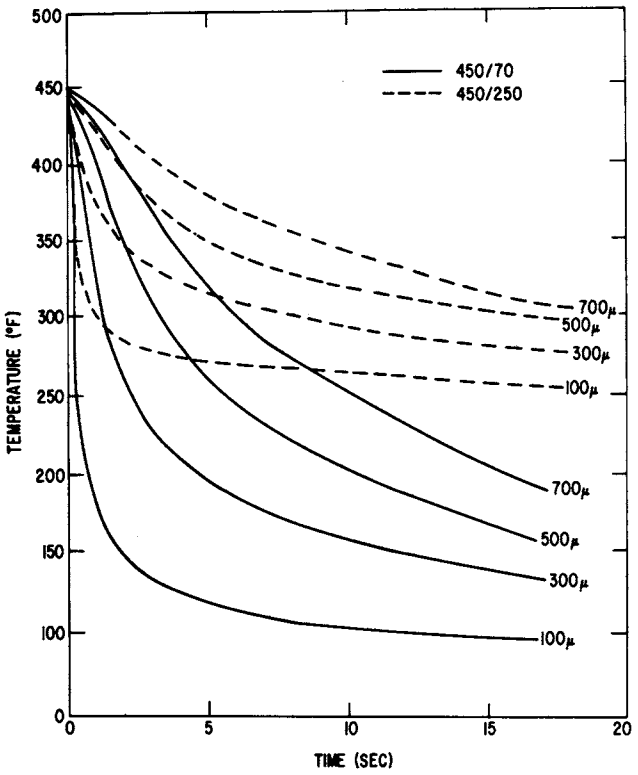

Fig. 6. Calculated cooling profiles at different distances from the surfaces of samples 450/70 and 450/250.

sharply in the outer 200 μ of the samples. This rapid drop undoubtedly reflects the steep temperature gradient set up in this region during molding.

In Figure 6 we present a theoretical time–temperature plot for samples molded at a melt temperature of 450°F and mold temperatures of 70 and 250°F. The calculation is carried out after the method of Carslaw and Jaeger and assumes the sample is a finite slab and that no crystallization takes place (a reasonable assumption for the highly amorphous skin).[10] The gradients are calculated from the infinite series

$$\frac{T_1 - T}{T_1 - T_0} = 2 \sum_{n=0}^{\infty} \frac{(-1)^n}{(n + 1/2)\pi} \cos (n + 1/2) \frac{\pi y}{b} \exp. - (n + 1/2)^2 \pi^2 \frac{\alpha t}{b^2} \quad (1)$$

in terms of dimensionless temperature $(T_1 - T)/(T_1 - T_0)$, dimensionless length (y/b), and dimensionless time $(\alpha t/b^2)$ as defined in the reference. The thermal conductivity, heat capacity, and density at 240°C were taken as 3.36×10^{-4} cal/cm sec deg, 0.4639 cal/g°C, and 1.22 g/cm^3, respectively.

Figure 6 indicates that the outer 100–300 μ of the bars approach the mold temperature within seconds after injection. In the 450/70 sample the skin is quenched to near the glass temperature (35°C) in 1–2 sec and the lowest measured skin density (1.2811 g/cm^3) is correspondingly close to the amorphous density (1.2782 g/cm^3) determined from thin-film studies.[11] As expected, all samples cool slowly in the core regions, thus accounting for the relatively constant core densities.

The fractional crystallinities of the four 450°F samples are indicated on the right axis of Figure 5. These values were calculated from the equation

$$w_c = \frac{\rho_c(\rho - \rho_a)}{\rho(\rho_c - \rho_a)} \tag{2}$$

where ρ_a is the amorphous density (1.278 g/cm^3) and ρ_c is the α crystalline density determined by Boye (1.396 g/cm^3).[12] The reader will note that the values are low for such a rapidly crystallizing polymer indicating that a large fraction of the material may be incorporated in chain folds, loops, and tie molecules. Molecular models show, for example, that a rather large section of the bulky PBT molecule must be involved in each chain fold. This observation suggests that the maximum lamellar crystallinity may be substantially less than that calculated from unit-cell parameters.

X-Ray Diffraction Studies

Wide-angle x-ray diffraction patterns taken on seetions cut parallel and perpendicular to the flow direction showed typical Debye-Scherrer rings which could be indexed to the unit cell of the α crystal form of poly(butylene terephthalate).[12] The observed and calculated d-spacings are presented in Table II. No reflections characteristic of the all trans β form could be identified. Photographs of patterns taken successively closer to the sample exteriors showed decreased intensity and increased line broadening associated with diminished crystallinity. Only amorphous halos were recorded for all samples at depths of 20 μ or less. There was no evidence of arcing in any of the patterns. Characteristic diffraction patterns taken on sections cut parallel to the flow direction and approximately 75 and 600 μ from the skin of sample 450/70 are shown in Figures 7a and 7b.

TABLE II
Observed and Calculated d-Spacings for Poly(butylene Terephthalate)
Triclinic unit cell

a = 4.83 Å	α = 99.9
b = 5.95 Å	β = 64.6
c = 11.67 Å	γ = 69.4

I/I_0	d (measured)	d (calculated)	hkl
mw	9.74	9.7	001
ms	5.54	5.50	$10\bar{1}$
s	5.10	5.15	010
m	4.32	4.28, 4.33	$1\bar{1}\bar{1}$, $10\bar{2}$
w	4.20	4.18	$1\bar{1}0$
w	3.95	3.97	011
vs	3.80	3.70, 3.83	$1\bar{1}\bar{2}$, 100
vs	3.53	3.59, 3.51, 3.39	$10\bar{3}$, $02\bar{1}$, $01\bar{2}$
vw	3.05	3.25	003
w	2.85	2.91	$11\bar{3}$
vw	2.75	2.76, 2.73	$02\bar{1}$, $12\bar{1}$
vvw	2.61	2.57	020
vw	2.425	2.44	$12\bar{2}$, $2\bar{1}\bar{2}$, $1\bar{1}\bar{4}$, 021
w	2.28	2.34, 2.29, 2.25	$2\bar{1}\bar{1}$, $10\bar{5}$, $02\bar{4}$
w	2.165	2.15, 2.16	$2\bar{1}\bar{4}$, $2\bar{1}0$

(a)

(b)

Fig. 7. Wide-angle diffraction patterns of samples taken (a) 75 μ from the skin and (b) 600 μ from the skin of sample 450/70.

Notched Izod Tests

The notched Izod strengths of bars having both molded and cut notches are presented in Table III together with their respective mold and melt temperatures. Each value represents an average of 15 tests. Brittle fractures were observed in all cases. A steady increase in impact strength with skin thickness is observed with samples molded from the 450°F melt showing consistently higher impact strengths than those obtained from the 510°F melt. These variations are not the result of variations in overall sample crystallinities which are very

TABLE III
Notched Izod Strengths of Injection Molded Poly(butylene Terephthalate) Samples

	Melt temperature, °F	Mold temperature, °F	Average density, g/cm³	Notched Izod Strength ft lb per inch of notch
Molded notch	450	70	1.3032	1.8
		122	1.3034	1.4
		194	1.3059	1.2
		250	1.3070	1.1
	510	70	1.3012	1.3
		122	1.3025	1.3
		194	1.3026	1.1
		250	1.3070	0.9
Cut notch	450	70		0.9
		122		0.8
		194		0.9
		250		0.8
	510	70		0.9
		122		0.9
		194		0.8
		250		0.7

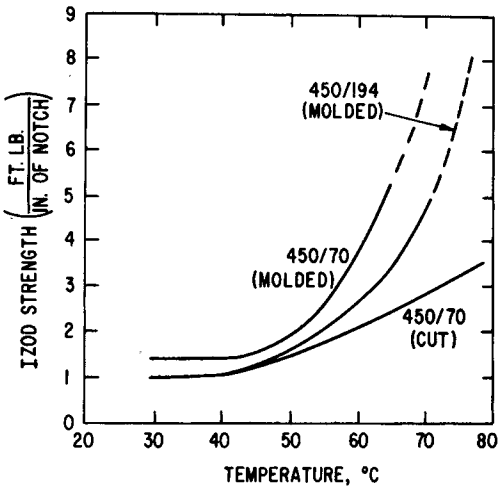

Fig. 8. Variation in impact strength with temperature for samples 450/70 and 450/194 (molded notches) and for 450/70 (cut notches).

small (see Table III). All samples with cut notches showed consistently lower impact strengths than those with molded notches. The impact strengths of specimens with cut notches did not vary significantly with processing temperature.

The variation in impact strength with testing temperature is shown in Figure 8 for samples fabricated at several different molding temperatures and for those with cut notches. The impact strengths are seen to rise sharply ~20°C above the glass temperature, with several samples tested at 70–75°C showing no break at 10 ft lb per inch of notch. Again the samples with thicker skins showed consistently higher notched Izod strengths than those with thinner skins or with

cut notches. Moreover, a downward displacement of ~10°C in the "ductile-brittle" transition was noted in samples molded at lower mold temperatures.

Fracture Surface Morphology

All of the impact bars tested at room temperature failed in a brittle manner. In each case an elliptical mirror could be observed hear the center of the notch slightly below the notch tip. The mirror was readily resolved in the optical microscope and was found to be roughly constant in size and to move steadily inward with decreasing mold temperature and increasing skin thickness. The migration of the mirror zone away from the notch is readily visible in the fracture surface micrographs in Figures 9a–9d. The dimensions of the primary failure zones and distances from the notch are presented in Table IV. We feel that cohesive failure initiates at the mirror and is followed by rapid crack propagation through the rest of the sample.

An SEM photograph of the fracture surface of a notched Izod bar (sample 450/250) is presented in Figure 10. With the exception of the mirror-zone displacement the essential morphological features are relatively unchanged in specimens molded at other temperatures. The base of the notch and the mirror zone are visible on the left hand side of the figure. The higher magnification photograph in Figure 11 shows that the mirror is relatively smooth and is completely surrounded by a sharply undulating plateau-like fracture surface. This symmetrical morphology suggests that the fracture is propagated back toward the notch tip as well as forward into the sample.

Transmission electron micrographs of replicas of this region show a number of details which are not readily visible in the SEM and which are surprisingly similar to features described for polycarbonate undergoing brittle fracture. Large areas in the cohesive failure zone appear smooth to a magnification of 100,000×. Just outside this area, however, one sees the beginnings of a patch structure commonly associated with craze material formed during biplanar crack propagation through a glassy material.[13] This feature can be observed on the lower right hand side of Figure 12 which was taken near the edge of the mirror zone. Still further away, the fully developed mackerel pattern observed in both polystyrene and polycarbonate fracture surfaces[13,14] can be seen as shown in Figure 13. This feature is also associated with biplanar crack propagation and usually occurs in well-defined bands concentric about the origin of fracture. In the PBT samples the mackerel structure is on a smaller scale and less continuous than in polycarbonate. We believe that the pattern may be broken up by pref-

TABLE IV
Size and Position of Primary Failure Zone in Poly(butylene Terephthalate) Impact Bars

	Mold temperature, °F	Melt temperature, °F	Area of failure, zone $\mu^2 \times 10^{-4}$	Distance from notch tip, μ
Molded notch	450	70	4.45	450
		122	3.80	385
		194	5.42	320
		240	5.65	220
Cut notch (independent of molding conditions)			4.46	200

erential fracture around spherulite or lamellar boundaries. Occasional fibrils can be seen drawn out from the patches.

Between the patches in Figure 13 a pronounced nodular structure can be observed. An enlargement of such an area is shown in Figure 14. The nodules are

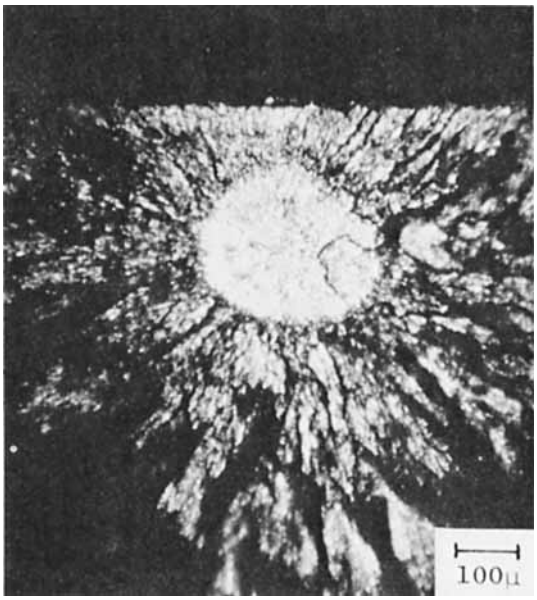

(a)

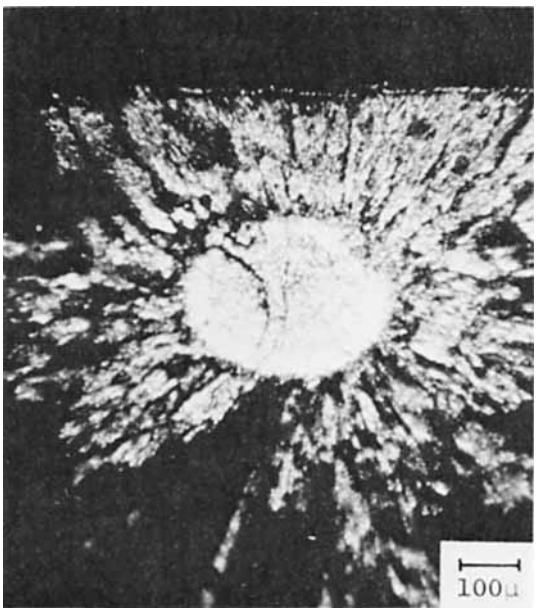

(b)

Fig. 9 (*continued*)

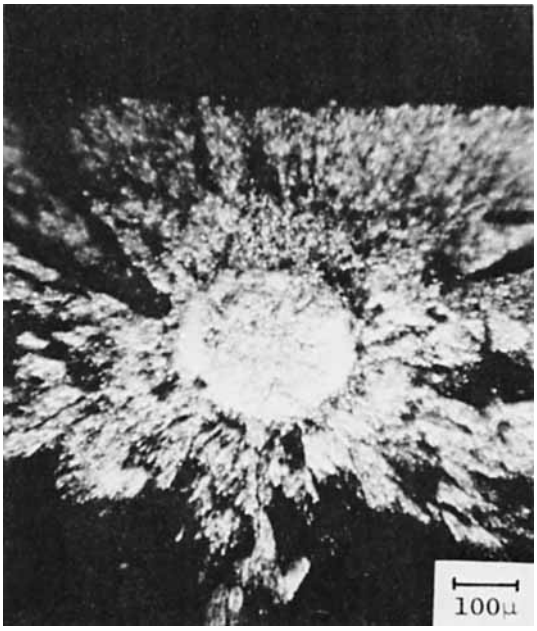

(c)

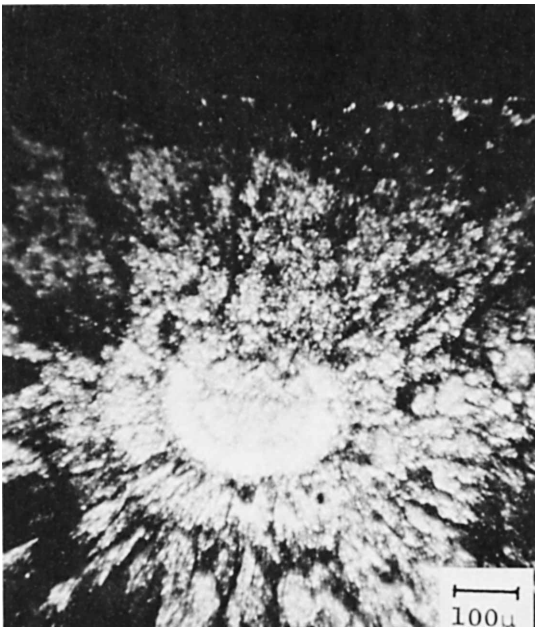

(d)

Fig. 9. Optical micrographs, incident steep illuminations of cohesive failure mirror in samples (a) 450/250, (b) 450/194, (c) 450/122, and (d) 450/70. All samples gold coated. The notch tips are at the tops of the photographs.

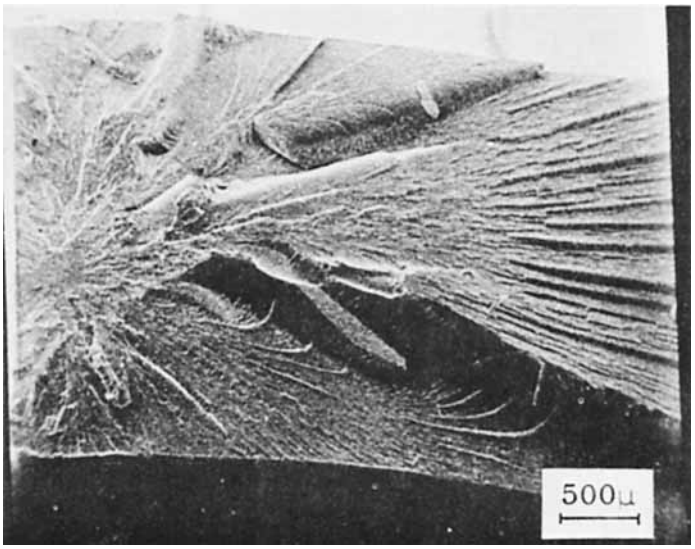

Fig. 10. SEM photograph showing typical fracture surface in a notched Izod bar from sample 450/250 broken at room temperature. The notch tip is on the left.

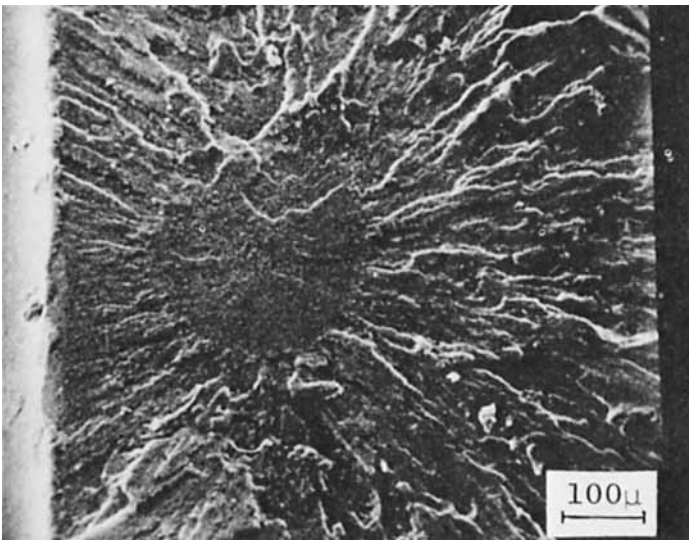

Fig. 11. Higher magnification photograph of mirror zone in Figure 10.

~1.0 μ in diameter. It has been suggested that the nodules may be collapsed fibrils of craze material which result when a crack is driven through a crazed region.[15] The small strands occasionally observed between the nodules indicate that films as well as fibrils of material are drawn out during the fracture process.

Substantial changes in fracture surface morphology were observed in samples broken at elevated temperatures. As might be expected, drawing played an increasingly important role in the fracture with considerable inward deformation of the sides of the impact bars observed at 50°C. The mirror zone moved inward with test temperature, first becoming less distinct on the side away from the

Fig. 12. Transmission electron micrograph of replica of PBT fracture surface. The smooth region of cohesive failure is visible at the upper left and the beginnings of patch fracture on the lower right.

notch and eventually disappearing completely. This behavior is associated with increasing shear deformation at the notch tip prior to fracture.

A SEM photograph of a poly(butylene terephthalate) bar fractured at 70°C and showing the features described above is presented in Figure 15. While at first glance the drawn regions appear to be smooth, higher magnification photographs reveal that the entire surface is highly rippled with a very regular period

Fig. 13. Transmission electron micrograph of replica of PBT fracture surface. This area is ~200 μ from the mirror zone and shows a characteristic mackerel fracture pattern and numerous small nodules of residual craze material.

of ~5 μ as shown in Figure 16. The large discontinuities in the band structure noted on lower temperature fracture surfaces (see Fig. 13) are generally absent. The bands are attributed to oscillations of the elastic shock wave preceeding the rapidly advancing crack tip as noted by Murray and Hull for polystyrene, although the band spacing in poly(butylene terephthalate) is substantially smaller. Shreds of material could be seen torn from the tops of some of the ripples. These shreds showed considerable birefringence when viewed in reflected polarized light, although the ripples themselves were not birefringent.

Fig. 14. Transmission electron micrograph of replica of PBT fracture surface. An enlargement of the nodular area in Figure 12 is shown.

This observation was somewhat surprising since craze material differs in refractive index from the bulk polymer and should show up as bright bands in the microscope. The absence of birefringence suggests the craze layer must be very thin or has undergone significant relaxation after fracture.

High-Speed Stress–Strain Measurements

Typical load–elongation curves for bars broken in the MTS machine at test speeds of 20 msec/in. (with and without damping) and 200 msec/in. are presented

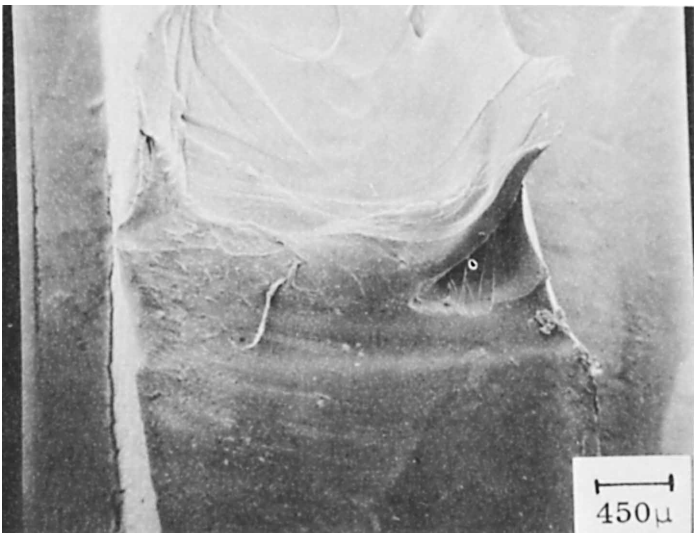

Fig. 15. SEM photograph of a fracture surface of a notched Izod bar from sample 450/70 broken at 70°C. The notch face is at the bottom of the photograph.

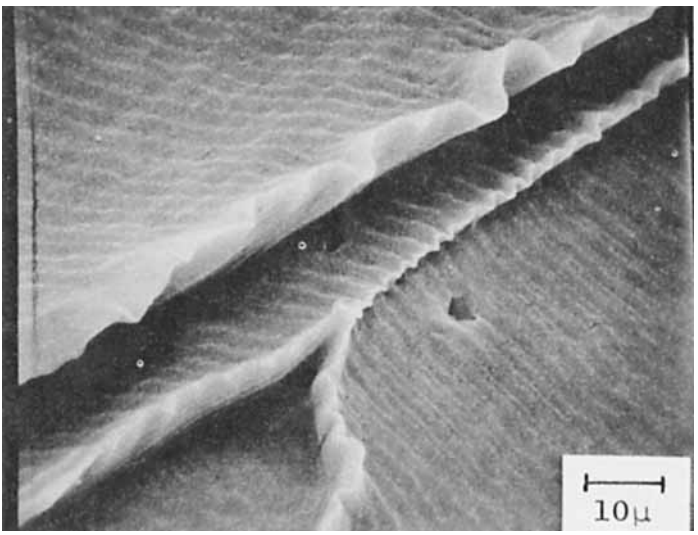

Fig. 16. Higher magnification photograph of Figure 15 showing regular ripples on the surface.

in Figures 17a–17c. The more pronounced secondary oscillations shown in Figure 17a arise from the 8000-cps ring developed in the ram on impact. The effectiveness of the damping material in reducing the ring at high test speeds is obvious in comparing Figures 17a and 17b. The reader will note that there is no evidence of yielding or plastic deformation of the bars prior to fracture, although the slight nonlinearity of the load–elongation curve indicates that there is some nonelastic component to the strain. This may be associated with craze development prior to fracture, but these details have not been resolved.

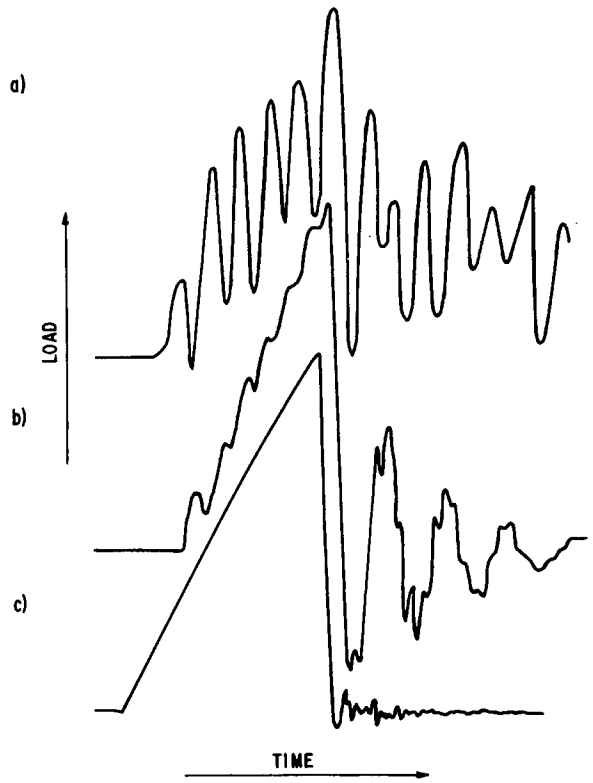

Fig. 17. Load–elongation curves for samples 450/70 broken at (a) 20 msec/inch (no damping), (b) 20 msec/inch (damped), and (c) 200 msec/inch (no damping).

The fracture load, maximum deflection, and energy to break for samples 450/70 and 450/194 are plotted as functions of test speed in Figures 18a–18c. In all cases larger values were obtained with samples molded at the lower mold temperatures. For samples molded at a given temperature, the fracture load was found to be insensitive to rate over the range of test speeds employed, while the maximum deflection increased with decreasing rate. Thus at constant test speed the increase in fracture energy with decreasing mold temperature arises from increases in both deflection and load at fracture, while the increase in fracture energy with decreasing testing speed at constant mold temperature arises primarily from an increase in maximum deflection.

On the left hand side of Figure 18c are values for fracture energy calculated from notched Izod data (see Table III). Although the stress configuration is quite different in the two tests, the agreement in the values indicates that the fracture processes are very similar and that low-speed test data can be successfully extrapolated to impact speeds. Microscopic examination of the fracture surfaces of samples broken at 20 msec/in. showed the familiar mirror and radiating-crack pattern described earlier. The inward displacement of the mirror with lower mold temperature was noted. At lower test speeds the mirror zone in both samples became less well defined as observed in Izod samples which fractured in a brittle manner at 40–50°C. The time–temperature superposition

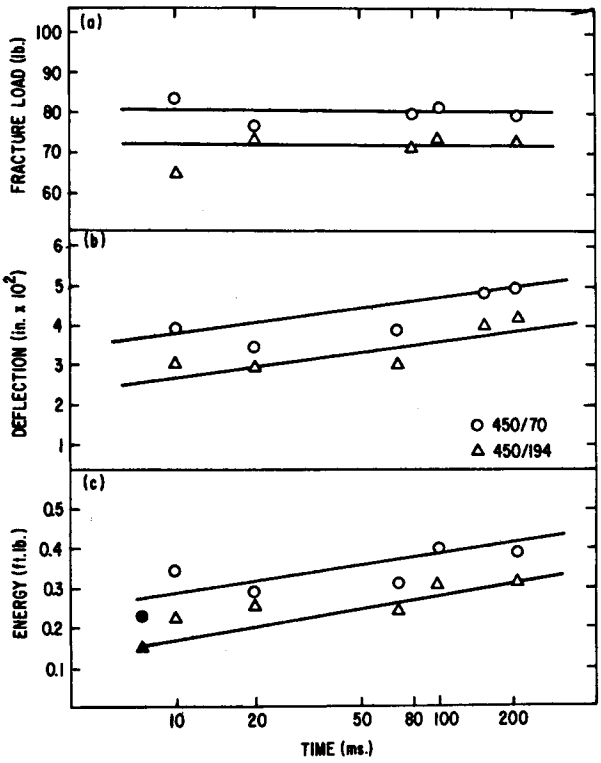

Fig. 18. Plots showing (a) fracture stress, (b) deflection, and (c) energy to break as a function of test speed for samples 450/70 and 450/194. The solid data points in c are calculated from notched Izod data.

characteristics of the fracture process are currently being explored more fully and will be reported on in a future paper.

DISCUSSION

A precise description of the local stress–strain criteria which precipitate failure in isotropic, notched samples is not yet available. However, notch sensitivity is commonly described in terms of the development of a triaxial stress at the notch tip with brittle failure occurring as a result of the transition from plane stress to plane strain condition as the sample is deformed.[16,17] LeGrand has noted in three-point bending tests of Lexan polycarbonate that failure initiates from a Griffith type flaw which develops in the area of maximum stress concentration $\sim$160 μ below the notch tip.[18] In brittle failure the flaw continues to increase in size with increasing stress until the sample fails catastrophically as the flaw approaches the surface. Ductile failure, in contrast, is accompanied by inward collapse of the walls to produce a three-dimensional void after the flaw reaches a diameter of $\sim$0.01 cm. More recent evidence indicates that crazing may play an important role in the brittle fracture of polycarbonate.[14]

In PBT specimens with molded-in notches the stress field during impact fracture is further complicated by the presence of an anisotropic skin while the opacity of the crystalline specimens precludes observation of the development of crazes and internal flaws. Therefore we present a quantitative description of the

fracture process based on the characteristics of the fracture surface as well as the observed stress–strain behavior.

Under impact conditions, bars with no skins or with very thin skins fracture cohesively in plane strain at a point ~200 μ below the notchtip. This is slightly below the point of maximum stress concentration calculated by LeGrand for isotropic Lexan polycarbonate samples. Maximum deflection at fracture is less than 0.03 in. and the highly linear load–elongation curves suggest that there is very little crazing or plastic flow before break. The radial crack pattern surrounding the mirror zone indicates that rapid crack propagation occurs back toward the notch tip as well as forward through the sample.

As the thickness of the low-modulus skin is increased, the transition from plane stress to plane strain is delayed as a result of the greater deformability of the material at the notch tip. The maximum deflection at break is increased to 0.04 in. and the maximum load also rises since a greater volume of deformed material develops beneath the notch tip as the incipient primary failure zone is displaced inward. As noted above the size of the cohesive failure mirror remains relatively constant, indicating that the maximum local stress in this region at break does not change appreciably with skin thickness. Again the stress–strain curves reveal little evidence of crazing prior to fracture. The small amounts of craze material observed on the fracture surface are believed to be associated with crazes developing immediately ahead of the crack at the time of fracture.

Above 50°C the molded specimens begin to fail in a ductile manner with a sharp rise in impact strength and extensive shear deformation at the notch tip. Although load–elongation data at elevated temperatures are not yet available, examination of the fracture surfaces indicates that the samples deform by yielding until, very close to the fracture point, the yield stress exceeds the craze stress and the sample crazes and breaks. Craze remnants are left on top of the drawn fracture surface. The absence of a cohesive failure mirror indicates that failure occurs prior to the transition of plane strain. In samples where the skin thickness is reduced and the modulus is higher at the notch tip the craze stress is exceeded at lower strain and the ductile–brittle transition is displaced downward in temperature as shown in Figure 8.

CONCLUSIONS

1. Injection-molded articles of poly(butylene terephthalate) develop a nonspherulitic skin which may vary from 20 to 200 μ in thickness depending on melt and mold temperature. A continuous density increase occurs in this region with the fractional crystallinity of the core approaching 0.25. The degree of orientation is low and the complicated multiple-zone morphologies reported in other systems are absent.

2. The Izod impact strengths of bars with molded-in notches are very sensitive to skin thickness increasing from 0.8 to 1.8 ft lb per inch of notch as the skin thickness increases from 0 to 200 μ. High-speed stress–strain data show that the higher impact strengths result from increases in both load and deformation at fracture. A ductile–brittle transition at impact speeds is observed at 50°C.

3. The fracture surfaces of bars broken under impact at room temperature show a relatively smooth cohesive failure mirror and radiating-crack pattern. The mirror remains approximately constant in size but moves inward with in-

creasing skin thickness and disappears at lower test speeds or higher temperatures. Craze remnants are observed on the fracture surfaces under all conditions but crazing does not appear to contribute to energy dissipation during most of the deformation.

4. At room temperature the bars appear to fail in plane strain and there is no evidence of plastic deformation near the exterior of the lateral faces of the bar or near the notch tip. The load–elongation curves are nearly linear. At higher temperatures significant shear yielding occurs until the critical stress for crazing is exceeded and then the bars fail by a craze–crack mechanism. In each case failure is delayed as the surface skin increases in thickness.

The authors are indebted to A. F. Yee for providing valuable thoughts and criticisms during this study and for his generous donations of time and equipment.

References

1. B. Maxwell, *J. Polym. Sci. C*, **9**, 43 (1965).
2. T. W. Haas and B. Maxwell, *Polym. Eng. Sci.*, **9**, 225 (1969).
3. R. J. Barriault and L. F. Gronholz, *J. Polym. Sci.*, **18**, 393 (1955).
4. D. R. Fitchman and Z. Mencik, *J. Polym. Sci.*, **11**, 951 (1973).
5. M. R. Kantz, H. D. Newmann, Jr., and F. H. Stigale, *J. Appl. Polym. Sci.*, **16**, 1249 (1972).
6. E. S. Clark, *SPE J.*, **23**, 46 (1967).
7. E. S. Clark, *Appl. Polym. Sym.*, **20**, 325 (1973).
8. E. R. Dixon and J. B. Jackson, *J. Materials Sci.*, **3**, 464 (1968).
9. L. H. Tung and W. C. Taylor, *J. Polym. Sci.*, **21**, 144 (1956).
10. H. S. Carslaw and J. C. Jaeger, *Conduction of Heat in Solids*, Oxford University Press, 1959 p. 101–000.
11. A. R. Shultz and L. D. Stang, unpublished data, GE Research and Development Corp., Schenectady,
12. C. A. Boye, Jr. and J. R. Overton, "A Reversible, Stress-Induced Solid Phase Transition in Poly(tetramethylene Terephthalate)," paper presented at the ACPS meeting, Division of High Polymers, Philadelphia, March 1974.
13. J. Murray and D. Hull, *Polymer*, **10**, 451 (1969).
14. D. Hull and T. W. Owen, *J. Polym. Sci. A-2*, **11**, 2039 (1973).
15. R. N. Haward and I. Brough, *Polymer*, **10**(9), 724 (1969).
16. I. M. Ward, *Mechanical Properties of Solid Polymers*, Wiley, 1971, pp. 336–340.
17. A. F. Yee and W. V. Olszewski, "Plane Strain and the Brittleness of Plastics," paper to be presented at the ACS Symposium on the Toughness and Brittleness of Plastics in Atlantic City, N.J., September 1974.
18. D. G. LeGrand, *J. Appl. Polym. Sci.*, **13**, 2129 (1969).

Received January 3, 1975